# On the optimality of the spherical Mexican hat wavelet estimator for the primordial non-Gaussianity

A. Curto,[1][*] E. Martínez-González,[1] R. B. Barreiro[1]

[1] *Instituto de Física de Cantabria, CSIC-Universidad de Cantabria, Avda. de los Castros s/n, 39005 Santander, Spain.*

**ABSTRACT**

We study the spherical Mexican hat wavelet (SMHW) as a detector of primordial non-Gaussianity of the local type on the Cosmic Microwave Background (CMB) anisotropies. For this purpose we define third order statistics based on the wavelet coefficient maps and the original map. We find the dependence of these statistics in terms of the non-linear coupling parameter $f_{nl}$ and the bispectrum of this type of non-Gaussianity. We compare the analytical values for these statistics with the results obtained with non-Gaussian simulations for an ideal full-sky CMB experiment without noise. We study the power of this method to detect $f_{nl}$, i. e. the variance of this parameter $\sigma^2(f_{nl})$, and compare it with the variance obtained from the primary bispectrum for the same experiment. Finally we apply our wavelet based estimator on WMAP-like maps with incomplete sky and inhomogeneous noise and compare with the optimal bispectrum estimator. The results show that the wavelet cubic statistics are as efficient as the bispectrum as optimal detectors of this type of primordial non-Gaussianity.

**Key words:** methods: data analysis - cosmic microwave background

## 1 INTRODUCTION

The primordial perturbations generated during the inflationary period are imprinted in the radiation and matter distribution. The study of the CMB anisotropies has become an important source of information to understand the physics of the very early universe. Thus for example the search of primordial non-Gaussianities on the CMB anisotropies, the measurement of the tilt and running of the index of the power spectrum $\Delta_{\mathcal{R}}^2(k) = Ak^{n_s-1}$ and the search of primordial gravitational waves have become part of a set of observables that are being used to select among many different models for the inflationary paradigm. The simplest models of inflation as the standard, single-field, slow roll inflation (Guth 1981; Albrecht & Steinhardt 1982; Linde 1982, 1983; Mukhanov et al. 1992) predict that the anisotropies are compatible with a nearly Gaussian random field.

There are two main procedures for the Gaussianity analyses of a map of CMB anisotropies. One can perform blind tests searching for deviations with respect to the null hypothesis (the random field is Gaussian). The second option is to consider different physical scenarios and to look for their imprints on the anisotropies.

Among the many different blind tests performed on the *Wilkinson Microwave Anisotropy Probe* WMAP[1] data, there are several reports of anomalies present in these data. We can mention the asymmetry between the two ecliptic hemispheres (Eriksen et al. 2004; Hansen et al. 2004; Eriksen et al. 2005, 2007; Hoftuft et al. 2009; Pietrobon et al. 2010; Vielva & Sanz 2010b), anomalous quadrupole-octupole alignment (Copi et al. 2004; de Oliveira-Costa et al. 2004; Copi et al. 2006; Gruppuso & Burigana 2009; Frommert & Enßlin 2010), a non-Gaussian cold spot (Vielva et al. 2004; Mukherjee & Wang 2004; Cruz et al. 2005, 2006, 2007a,b, 2008; Vielva et al. 2010a), unexpected alignment of CMB structures (Wiaux et al. 2006; Vielva et al. 2007) and an unexpected low value of the CMB variance (Monteserín et al. 2008; Cruz et al. 2010).

Regarding targeted tests, one has to think about the possible physical mechanisms that lead to non-Gaussianities and search for their possible signatures. Historically motivated, many inflationary models that generate non-Gaussianity can be parametrised by the local non-linear coupling parameter $f_{nl}$, which is introduced through the primordial gravitational potential (Verde et al. 2000; Komatsu & Spergel 2001; Bartolo et al. 2004)

[*] e-mail: curto@ifca.unican.es

[1] http://map.gsfc.nasa.gov/

$$\Phi(\mathbf{x}) = \Phi_L(\mathbf{x}) + f_{nl}\{\Phi_L^2(\mathbf{x}) - \langle \Phi_L(\mathbf{x}) \rangle^2\}. \qquad (1)$$

Significant non-Gaussianity of the local form can be generated for example in the curvaton model (Lyth et al. 2003), multi-field inflationary models (Komatsu et al. 2005), the inhomogeneous reheating scenario (Dvali et al. 2004; Bartolo et al. 2004), models with low reheating efficiency (Mukhanov et al. 1992; Salopek & Bond 1990), models based on hybrid inflation (Lin 2009), etc. This kind of non-Gaussianity is characterised by correlations among modes $k$ in the Fourier space with very different amplitude (Creminelli et al. 2006, 2007). This can be seen for example through the shape function $F(k_1, k_2, k_3)$ of the local non-Gaussianity

$$F(k_1, k_2, k_3) = A f_{nl} \left( \frac{1}{k_1^3 k_2^3} + \frac{1}{k_1^3 k_3^3} + \frac{1}{k_2^3 k_3^3} \right) \qquad (2)$$

where $A$ is a normalization constant (see for example the plot of the shape function of the local distribution by Babich et al. 2004). The most significant contributions of this kind of non-Gaussianity arise for the cases with $k_1 << k_2 \approx k_3$ and permutations among the three modes $k_1$, $k_2$ and $k_3$. Other shapes of inflationary models that produce their particular kind of non-Gaussianity are for example the *equilateral* and the *orthogonal* shape (Senatore et al. 2010; Komatsu et al. 2010). The most significant contribution to the non-Gaussianity is located in specific ranges of the Fourier space $k_1 \approx k_2 \approx k_3$ for the *equilateral* shape whereas the *orthogonal* shape is nearly orthogonal to the two previous forms.

In this paper we focus on the non-Gaussianity of local type. The canonical inflationary model predicts $f_{nl} \sim 10^{-2}$ whereas other models predict larger amounts of non-Gaussianity (Bartolo et al. 2004). An eventual detection of a deviation from Gaussianity will rule out many inflationary models from the present available list. Many studies have been performed to constrain the local $f_{nl}$ on different data sets such as the *Cosmic Background Explorer (COBE)* data (Komatsu et al. 2002; Cayón et al. 2003a), the MAXIMA data (Santos et al. 2003; Cayón et al. 2003b), the *Very Small Array* data (Smith et al. 2004), the BOOMERang data (De Troia et al. 2007; Natoli et al. 2009) and the Archeops data (Curto et al. 2007, 2008). Significant improvements on the $(S/N)$ ratio of the local $f_{nl}$ parameter have been achieved with the WMAP data using different estimators. For most of the works, $f_{nl}$ is positive with a significance between $1\sigma$ and $2\sigma$. See for example the results obtained with different bispectrum-based estimators (Komatsu et al. 2003; Spergel et al. 2007; Creminelli et al. 2006, 2007; Yadav & Wandelt 2008; Komatsu et al. 2009; Smith et al. 2009; Elsner & Wandelt 2009; Bucher et al. 2010; Komatsu et al. 2010; Smidt et al. 2010), with the SMHW (Curto et al. 2009a,b), with needlets (Pietrobon et al. 2009; Rudjord et al. 2009, 2010; Cabella et al. 2010), with the HEALPix wavelet (Casaponsa et al. 2010), with the Minkowski functionals (Hikage et al. 2006; Gott et al. 2007; Hikage et al. 2008; Matsubara 2010), the N-PDF distribution (Vielva & Sanz 2009), the skewness of the power spectrum (Smidt et al. 2009), etc. Other works use the distribution of matter on large scales (see for example Dalal et al. 2008; Matarrese & Verde 2008; Slosar et al. 2008; Seljak 2009;

Desjacques & Seljak 2010; Xia et al. 2010) to constrain the local $f_{nl}$.

This work is a study of the efficiency of the third order wavelet-based estimators (Curto et al. 2009a,b) to detect primordial non-Gaussianity of the local type. We find the dependence of the third order estimators in terms of the local bispectrum and $f_{nl}$. We compare the power of this method to detect $f_{nl}$ with the optimal bispectrum estimator for an ideal full-sky and noiseless experiment and the same comparison for an experiment with WMAP 5-year and WMAP 7-year beam, noise and sky cut properties. Our results indicate that the wavelet estimators are as efficient as the optimal estimators based on the bispectrum.

The article is organised as follows. Section 2 presents the estimators based on wavelets, their dependence on the angular bispectrum, their analytical covariance matrix and the $f_{nl}$ Fisher matrix for wavelet and bispectrum estimators. In Section 3 we compare the $\sigma(f_{nl})$ values obtained with the wavelet estimator and the bispectrum estimator and the conclusions are presented in Section 4.

## 2   THE THIRD ORDER STATISTICS

### 2.1   Expected values of the wavelet estimator in terms of the bispectrum

The third order statistics of this analysis are based on the SMHW. See Antoine & Vandergheynst (1998); Martínez-González et al. (2002); Vielva (2007); Martínez-González (2008) for detailed information about the wavelets and a list of applications to the CMB anisotropies. Given a function $f(\mathbf{n})$ defined at a position $\mathbf{n}$ on the sphere and a continuous wavelet family on that space $\Psi(\mathbf{n}; \mathbf{b}, R)$, we define the continuous wavelet transform as

$$w(R; \mathbf{b}) = \int d\mathbf{n} f(\mathbf{n}) \Psi(\mathbf{n}; \mathbf{b}, R) \qquad (3)$$

where $\mathbf{b}$ is the position on the sky at which the wavelet coefficient is evaluated and $R$ is the scale of the wavelet.

Considering a set of different angular scales $\{R_i\}$ we define a third order statistic depending on three scales $\{i, j, k\}$ (Curto et al. 2009b)

$$q_{ijk} = \frac{1}{4\pi} \frac{1}{\sigma_i \sigma_j \sigma_k} \int d\mathbf{n} w(R_i, \mathbf{n}) w(R_j, \mathbf{n}) w(R_k, \mathbf{n}) \qquad (4)$$

where $\sigma_i$ is the dispersion of the wavelet coefficient map $w(R_i, \mathbf{n})$. In the particular case of $R_0 = 0$, $w(R_0, \mathbf{n}) \equiv f(\mathbf{n})$. Using the properties of the wavelet, we have

$$w(R_i, \mathbf{n}) = \sum_{\ell m} a_{\ell m} \omega_\ell(R_i) Y_{\ell m}(\mathbf{n}) \qquad (5)$$

and

$$\sigma_i^2 = \sum_\ell C_\ell \frac{2\ell + 1}{4\pi} \omega_\ell^2(R_i) \qquad (6)$$

where $\omega_\ell(R)$ is the window function of the wavelet at a scale $R$ and it is given by the harmonic transform of the mother wavelet of the SMHW (Martínez-González et al. 2002; Sanz et al. 2006). The convolution with the wavelet is equivalent to filter the maps with a window function $\omega_l(R)$ which depends on the scale. In Fig. 1 we plot the wavelet
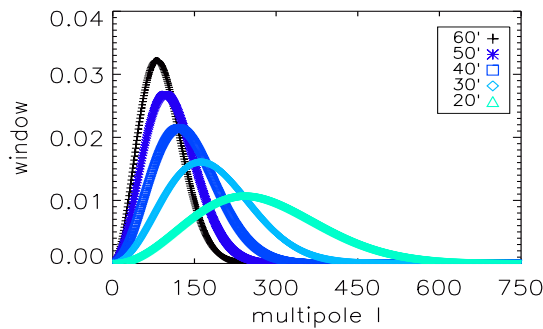
**Figure 1.** The window function for the SMHW at different angular scales. Note that the wavelet filters high multipoles for low angular scales and viceversa.

window function for several angular scales. For small scales, the wavelet filters low multipoles and viceversa. Therefore it is important to select a set of angular scales that ranges all the interesting multipoles.

### 2.2 The statistics and the primordial non-Gaussianity

Considering Eqs. 4 and 5, the third order moments can be written as

$$q_{ijk} = \frac{1}{4\pi} \frac{1}{\sigma_i \sigma_j \sigma_k}$$

$$\times \left\{ \sum_{\ell_1, \ell_2, \ell_3, m_1, m_2, m_3} a_{\ell_1 m_1} a_{\ell_2 m_2} a_{\ell_3 m_3} \right.$$

$$\times \omega_{\ell_1}(R_i) \omega_{\ell_2}(R_j) \omega_{\ell_3}(R_k)$$

$$\times \begin{pmatrix} \ell_1 & \ell_2 & \ell_3 \\ m_1 & m_2 & m_3 \end{pmatrix} \begin{pmatrix} \ell_1 & \ell_2 & \ell_3 \\ 0 & 0 & 0 \end{pmatrix}$$

$$\left. \times \sqrt{\frac{(2\ell_1 + 1)(2\ell_2 + 1)(2\ell_3 + 1)}{4\pi}} \right\}, \tag{7}$$

where matrix is the Wigner 3j symbol and we have used the Gaunt integral (Komatsu & Spergel 2001)

$$\int d^2\mathbf{n} Y_{\ell_1 m_1}(\mathbf{n}) Y_{\ell_2 m_2}(\mathbf{n}) Y_{\ell_3 m_3}(\mathbf{n}) =$$

$$\times \begin{pmatrix} \ell_1 & \ell_2 & \ell_3 \\ m_1 & m_2 & m_3 \end{pmatrix} \begin{pmatrix} \ell_1 & \ell_2 & \ell_3 \\ 0 & 0 & 0 \end{pmatrix}$$

$$\times \sqrt{\frac{(2\ell_1 + 1)(2\ell_2 + 1)(2\ell_3 + 1)}{4\pi}}. \tag{8}$$

The mean value of the third order statistic $q_{ijk}$ can be written in terms of the reduced bispectrum as defined by Komatsu & Spergel (2001):

$$\langle q_{ijk} \rangle = \frac{1}{4\pi} \frac{1}{\sigma_i \sigma_j \sigma_k}$$

$$\times \sum_{\ell_1, \ell_2, \ell_3} \omega_{\ell_1}(R_i) \omega_{\ell_2}(R_j) \omega_{\ell_3}(R_k) I^2_{\ell_1 \ell_2 \ell_3} b_{\ell_1 \ell_2 \ell_3}, \tag{9}$$

where $I_{\ell_1 \ell_2 \ell_3}$ is defined as

$$I_{\ell_1 \ell_2 \ell_3} =$$

$$\begin{pmatrix} \ell_1 & \ell_2 & \ell_3 \\ 0 & 0 & 0 \end{pmatrix} \sqrt{\frac{(2\ell_1 + 1)(2\ell_2 + 1)(2\ell_3 + 1)}{4\pi}}. \tag{10}$$

Now assuming a primordial gravitational potential of the form given by Eq. 1 it is possible to derive its corresponding bispectrum in terms of $f_{nl}$ (see Komatsu & Spergel 2001). The expected value of the third order moments is proportional to $f_{nl}$

$$\langle q_{ijk} \rangle_{f_{nl}} = \alpha_{ijk} \times f_{nl}, \tag{11}$$

where

$$\alpha_{ijk} = \frac{1}{4\pi} \frac{1}{\sigma_i \sigma_j \sigma_k}$$

$$\times \left\{ \sum_{\ell_1, \ell_2, \ell_3} \omega_{\ell_1}(R_i) \omega_{\ell_2}(R_j) \omega_{\ell_3}(R_k) I^2_{\ell_1 \ell_2 \ell_3} b^{prim}_{\ell_1 \ell_2 \ell_3} \right\}. \tag{12}$$

The pixel properties are taken into account by replacing $C_\ell$ by $C_\ell \left[ \omega_\ell^{(pix)} \right]^2$ in Eq. 6 and $b^{prim}_{\ell_1 \ell_2 \ell_3}$ by $b^{prim}_{\ell_1 \ell_2 \ell_3} \omega_{\ell_1}^{(pix)} \omega_{\ell_2}^{(pix)} \omega_{\ell_3}^{(pix)}$ in Eq. 12, where $\omega_\ell^{(pix)}$ is the pixel window function for the HEALPix pixelization (Górski et al. 2005).

We have evaluated the $\alpha_{ijk}$ statistics analytically using Eq. 12 as well as from non-Gaussian simulations for the same set of 12 angular scales used in Curto et al. (2009b)[2]. We have used a full-sky ideal experiment without noise and a characteristic angular resolution of 6.9 arcmin (HEALPix $N_{side} = 512$). We need the expected values of the local primordial bispectrum to evaluate analytically the statistics $\alpha_{ijk}$. We have computed the primordial bispectrum up to $\ell_{max} = 1535$ using the gTfast[3] code based on CMB-Fast (Seljak & Zaldarriaga 1996) to evaluate the transfer function. The cosmological parameters for this analysis are $\Omega_{cdm} = 0.25$, $\Omega_b = 0.05$, $\Omega_\Lambda = 0.70$, $\tau = 0.09$, $h = 0.73$ and a scale invariant spectral index $n = 1$ for the power spectrum $P(k)$. We have used a set of 300 non-Gaussian simulations generated with the same cosmological parameters following the algorithm defined in Liguori et al. (2003, 2007). The mean value of the $\alpha_{ijk}$ statistics of these simulations and its error bars are plotted in Fig. 2. These values are compared with the theoretical value obtained from Eq. 12. We can see that there is a good agreement between the simulations and the analytic model. There is a slight discrepancy at negative values but we do not consider it very significant due to the correlations among the $\alpha_{ijk}$ quantities. In any case, these values correspond to $\alpha_{ijk}$ involving large scales where cosmic variance is more important and a larger number of simulations would be needed to achieve convergence. There is also a slight deviation at small angular scales (corresponding to values of $\alpha_{ijk} \sim 0.5 \times 10^{-4}$). This may be related to numerical uncertainties in the evaluation of the integrals that lead to the bispectrum $b^{prim}_{\ell_1 \ell_2 \ell_3}$ at high multipoles $\ell$. However, we have seen that these small deviations do not introduce significant differences ($< 1\%$) in the estimation of $\sigma(f_{nl})$ when we use either the analytic or the simulated $\alpha_{ijk}$.

---

[2] The angular scales used in Curto et al. (2009b) are: 6.9, 10.6, 16.3, 24.9, 38.3, 58.7, 90.1, 138.3, 212.3, 325.8 and 500 arcmin. The unconvolved map was also included in the analysis.
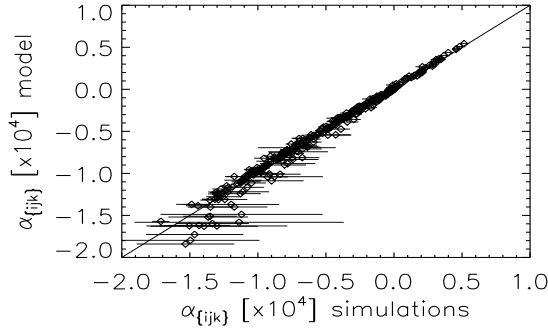[3] http://gyudon.as.utexas.edu/~komatsu/CRL/nongaussianity/

**Figure 2.** The $\alpha_{ijk}$ statistics computed analytically and with $n_{sim} = 300$ non-Gaussian simulations. The error bars correspond to the dispersion $\sigma(\alpha_{ijk})/\sqrt{n_{sim}}$ obtained with the simulations. The $\alpha_{ijk}$ are sorted such as the largest values correspond to pixel-dominated scales while the smallest values correspond to the largest scales.



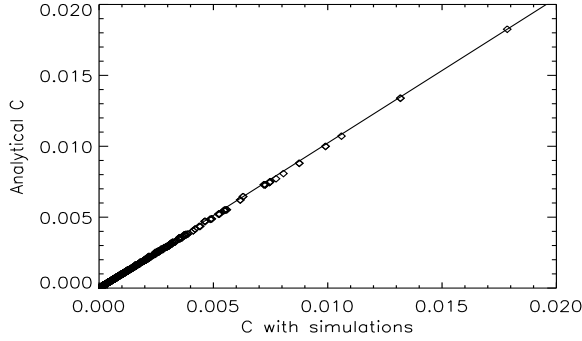**Figure 3.** The analytical covariance matrix computed through Eq. 16 compared to the one obtained from Gaussian simulations for the same power spectrum $C_\ell$.

### 2.3    The covariance of the third order statistics

The covariance matrix of the third order moments can be computed in the Gaussian limit using the properties of the covariance for the bispectrum. Considering the Gaussian case we have

$$C_{ijk,rst} = \langle q_{ijk}q_{rst}\rangle - \langle q_{ijk}\rangle\langle q_{rst}\rangle = \langle q_{ijk}q_{rst}\rangle. \tag{13}$$

From the definition of $q_{ijk}$

$$\langle q_{ijk}q_{rst}\rangle = \frac{1}{(4\pi)^2}\frac{1}{\sigma_i\sigma_j\sigma_k}\frac{1}{\sigma_r\sigma_s\sigma_t} \times \int \mathbf{d\hat{n}_1 d\hat{n}_2}$$
$$\times \big\langle w(R_i, \mathbf{n_1})w(R_j, \mathbf{n_1})w(R_k, \mathbf{n_1})$$
$$\times w(R_r, \mathbf{n_2})w(R_s, \mathbf{n_2})w(R_t, \mathbf{n_2})\big\rangle. \tag{14}$$

Using Wick's theorem and the properties of Gaussian distributions (in a similar manner as in Eq. 13 of Heavens 1998) we have

$$\big\langle w(R_i, \mathbf{n_1})w(R_j, \mathbf{n_1})w(R_k, \mathbf{n_1})$$
$$\times w(R_r, \mathbf{n_2})w(R_s, \mathbf{n_2})w(R_t, \mathbf{n_2})\big\rangle =$$
$$\langle w(R_i, \mathbf{n_1})w(R_j, \mathbf{n_1})\rangle$$
$$\times \langle w(R_k, \mathbf{n_1})w(R_r, \mathbf{n_2})\rangle$$

$$\times\langle w(R_s, \mathbf{n_2})w(R_t, \mathbf{n_2})\rangle +$$
$$+ permutations\ (total\ 15\ terms) \tag{15}$$

From these terms, there are only 6 that do not vanish in Eq. 14. They are those which involve the two coordinates $\mathbf{n_1}$ and $\mathbf{n_2}$ in the same average (Srednicki 1993). Taking this into account and the properties of the two point correlation functions (see Eq. 14 of Heavens 1998) we have

$$\langle q_{ijk}q_{rst}\rangle = \frac{1}{(4\pi)^2}\frac{1}{\sigma_i\sigma_j\sigma_k}\frac{1}{\sigma_r\sigma_s\sigma_t}\sum_{l_1l_2l_3}I_{l_1l_2l_3}^2 C_{l_1}C_{l_2}C_{l_3}$$
$$\times\{\omega_{l_1}(R_i)\omega_{l_1}(R_r)\omega_{l_2}(R_j)\omega_{l_2}(R_s)\omega_{l_3}(R_k)\omega_{l_3}(R_t)$$
$$+\omega_{l_1}(R_i)\omega_{l_1}(R_r)\omega_{l_2}(R_j)\omega_{l_2}(R_t)\omega_{l_3}(R_k)\omega_{l_3}(R_s)$$
$$+\omega_{l_1}(R_i)\omega_{l_1}(R_s)\omega_{l_2}(R_j)\omega_{l_2}(R_r)\omega_{l_3}(R_k)\omega_{l_3}(R_t)$$
$$+\omega_{l_1}(R_i)\omega_{l_1}(R_s)\omega_{l_2}(R_j)\omega_{l_2}(R_t)\omega_{l_3}(R_k)\omega_{l_3}(R_r)$$
$$+\omega_{l_1}(R_i)\omega_{l_1}(R_t)\omega_{l_2}(R_j)\omega_{l_2}(R_r)\omega_{l_3}(R_k)\omega_{l_3}(R_s)$$
$$+\omega_{l_1}(R_i)\omega_{l_1}(R_t)\omega_{l_2}(R_j)\omega_{l_2}(R_s)\omega_{l_3}(R_k)\omega_{l_3}(R_r)\} \tag{16}$$

The pixel properties are taken into account here by replacing $C_\ell$ by $C_\ell\omega_\ell^{(pix)}\omega_\ell^{(pix)}$. We have compared the analytical covariance matrix obtained through Eq. 16 with the covariance matrix obtained with $10^4$ Gaussian simulations for the same cosmological parameters defined in Subsect. 2.2. The covariance matrix elements $C_{ijk,rst}$, are compared by pairs in Fig. 3, obtaining a very good agreement.

### 2.4    $f_{nl}$ Fisher matrix of the third order moments

We discuss the detectability of primary non-Gaussianity with the third order moments. Assuming that the third order statistics are Gaussian-like, we can use the Gaussian likelihood to constrain the $f_{nl}$ parameter

$$L(f_{nl}) = C_0 e^{-\chi^2(f_{nl})/2}, \tag{17}$$

where $C_0$ is a constant and $\chi^2(f_{nl})$ is given by

$$\chi^2(f_{nl}) = \sum_{ijk,rst}(q_{ijk}^{obs} - \langle q_{ijk}\rangle_{f_{nl}})C_{ijk,rst}^{-1}(q_{rst}^{obs} - \langle q_{rst}\rangle_{f_{nl}}). \tag{18}$$

$C_{ijk,rst}^{-1}$ is the inverse of the covariance matrix of the third order statistics that we have computed analytically in the previous section, $q_{ijk}^{obs}$ are the third order statistics obtained from the data and $\langle q_{ijk}\rangle_{f_{nl}}$ are the expected values of the third order statistics for a given model with $f_{nl}$. As we have seen in Subsect. 2.2, $\langle q_{ijk}\rangle_{f_{nl}} = f_{nl}\alpha_{ijk}$, with $\alpha_{ijk}$ a constant independent of $f_{nl}$. Using this on Eq. 18, we have

$$\chi^2(f_{nl}) = \sum_{ijk,rst}(q_{ijk}^{obs} - \alpha_{ijk}f_{nl})C_{ijk,rst}^{-1}(q_{rst}^{obs} - \alpha_{rst}f_{nl}). \tag{19}$$

The variance of the $f_{nl}$ parameter can be computed using the Fisher matrix, which leads to:

$$\sigma^2(f_{nl}) = \frac{-1}{\frac{\partial^2 log L(f_{nl})}{\partial f_{nl}^2}} = \frac{1}{\frac{1}{2}\frac{\partial^2\chi^2(f_{nl})}{\partial f_{nl}^2}} =$$
$$= \frac{1}{\sum_{ijk,rst}\alpha_{ijk}C_{ijk,rst}^{-1}\alpha_{rst}}. \tag{20}$$

## 2.5 Principal Component Analysis of the third order moments

One of the most significant advantages of the wavelet-based analysis for this type of non-Gaussianity is that we are able to reduce the non-Gaussian information present in the bispectrum $b_{\ell_1\ell_2\ell_3}$ (about $10^7$ elements) to a set of several hundreds of $q_{ijk}$ statistics. However, these quantities are correlated and in certain conditions their covariance matrix may be ill-conditioned. There are different approaches to deal with these matrices. We will apply a Principal Component Analysis (PCA) in all the tests where the wavelet coefficient covariance matrix is involved in order to keep the errors related to the covariance matrix under a certain threshold.

The $\chi^2$ statistic of a random variable $\mathbf{x}$ of dimension $n$ can be written

$$\chi^2 = \sum_{i,j=1}^{n} x_i C_{ij}^{-1} x_j, \tag{21}$$

where $C$ is the covariance matrix of this variable. For any positive definite covariance matrix, it is possible to find a linear transformation of the $\mathbf{x}$ vector where the corresponding covariance matrix is the identity

$$\chi^2 = \sum_{i=1}^{n} y_i^2 \tag{22}$$

where $y_i = \sum_{j=1}^{n}(D^{1/2}R^t)_{ij}x_j$ and $D$ and $R$ are the eigenvalue and eigenvector matrices of the covariance matrix, $C = RDR^t$. In particular we sort the eigenvalues in descending order $D_i > D_{i+1}$. We can define a partial $\chi_m^2$ statistic

$$\chi_m^2 = \sum_{i=1}^{m} y_i^2 \tag{23}$$

such that only the $y_i$ quantities related to the largest $m$ eigenvalues are considered. The Fisher matrix for the $f_{nl}$ parameter using $\chi_m^2$ is defined as

$$\sigma_m^2(f_{nl}) \equiv \frac{1}{\frac{1}{2}\frac{\partial \chi_m^2(f_{nl})}{\partial f_{nl}^2}}. \tag{24}$$

As the third order moments are linearly proportional to $f_{nl}$, $x_j = q_j - f_{nl}\alpha_j$ and defining $\beta_i = \sum_{j=1}^{n}(D^{-1/2}R^t)_{ij}\alpha_j$, the Fisher matrix for the $f_{nl}$ parameter is

$$\sigma_m^2(f_{nl}) = \frac{1}{\sum_{i=1}^{m}\beta_i^2}. \tag{25}$$

## 2.6 Bispectrum estimator and error bars

The bispectrum-based estimators are the most widely applied tools for detecting primordial non-Gaussianity. Considering the angle averaged bispectrum $B_{\ell_1\ell_2\ell_3}$ as defined in Komatsu & Spergel (2001), it can be shown that the unbiased bispectrum-based minimum variance estimator for the full-sky limit and homogeneous noise is (Creminelli et al. 2006)

$$\hat{f}_{nl} = \frac{1}{N}\sum_{\ell_i,m_i}\begin{pmatrix}\ell_1 & \ell_2 & \ell_3\\ m_1 & m_2 & m_3\end{pmatrix}\frac{B_{\ell_1\ell_2\ell_3}^{model}}{C_{\ell_1}C_{\ell_2}C_{\ell_3}}$$
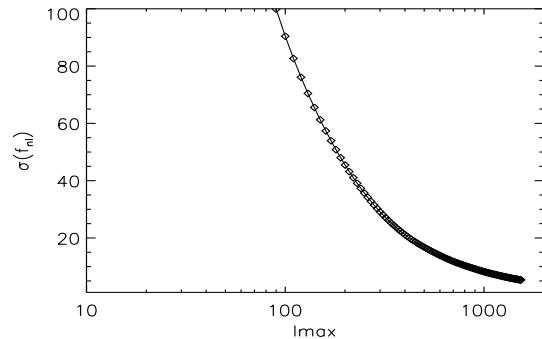$$\times a_{\ell_1 m_1}a_{\ell_2 m_2}a_{\ell_3 m_3}. \tag{26}$$



**Figure 4.** $\sigma(f_{nl})$ for different $\ell_{max}$ using the Fisher matrix of the bispectrum.

The unbiased bispectrum-based minimum variance estimator for the incomplete sky limit and inhomogeneous noise is (Creminelli et al. 2006)

$$\hat{f}_{nl} = \frac{1}{N}\sum_{\ell_i,m_i}\Bigg(\Big\langle a_{\ell_1 m_1}a_{\ell_2 m_2}a_{\ell_3 m_3}\Big\rangle_{f_{nl}=1}$$
$$\times C_{\ell_1 m_1,\ell_4 m_4}^{-1}C_{\ell_2 m_2,\ell_5 m_5}^{-1}C_{\ell_3 m_3,\ell_6 m_6}^{-1}$$
$$\times a_{\ell_4 m_4}a_{\ell_5 m_5}a_{\ell_6 m_6}$$
$$-3\Big\langle a_{\ell_1 m_1}a_{\ell_2 m_2}a_{\ell_3 m_3}\Big\rangle_{f_{nl}=1}$$
$$C_{\ell_1 m_1,\ell_2 m_2}^{-1}C_{\ell_3 m_3,\ell_4 m_4}^{-1}a_{\ell_4 m_4}\Bigg). \tag{27}$$

In particular, the signal-to-noise ratio for the $f_{nl}$ parameter, using a Fisher analysis for a full-sky and homogeneous noise experiment is (Komatsu & Spergel 2001)

$$\frac{f_{nl}}{\sigma^2(f_{nl})} = \sum_{2\leqslant\ell_1\leqslant\ell_2\leqslant\ell_3}\frac{B_{\ell_1\ell_2\ell_3}^{model}B_{\ell_1\ell_2\ell_3}^{model}}{\sigma_{\ell_1\ell_2\ell_3}^2}, \tag{28}$$

where $\sigma_{\ell_1\ell_2\ell_3}^2$ is the variance of the bispectrum.

Given a map with $N_{pix}$ pixels, the number of operations to obtain the local $f_{nl}$ through the KSW algorithm based on the bispectrum is $\sim 100N_{pix}^{3/2}$ (Komatsu et al. 2005). Our algorithm based on the SMHW requires $\sim n_{scal}N_{pix}^{3/2}$ operations, where $n_{scal}$ is the considered number of scales ($n_{scal} \sim 15$ for a WMAP-like experiment). Therefore, the wavelet algorithm is about an order of magnitude faster than the bispectrum algorithm for this kind of non-Gaussianity.

# 3 COMPARISON WITH THE OPTIMAL BISPECTRUM ESTIMATOR

In this Section we study the values of $\sigma(f_{nl})$ obtained with the wavelet and bispectrum estimators for a full-sky and homogeneous noise experiment and for WMAP-like 5-year and 7-year V+W combined maps.

## 3.1 Estimated error bars for $f_{nl}$ with an ideal experiment

We consider the local primordial bispectrum of a noiseless experiment with an angular resolution of 6.9 arc minutes ($\ell_{max} = 1535$), and a cosmological model characterised by
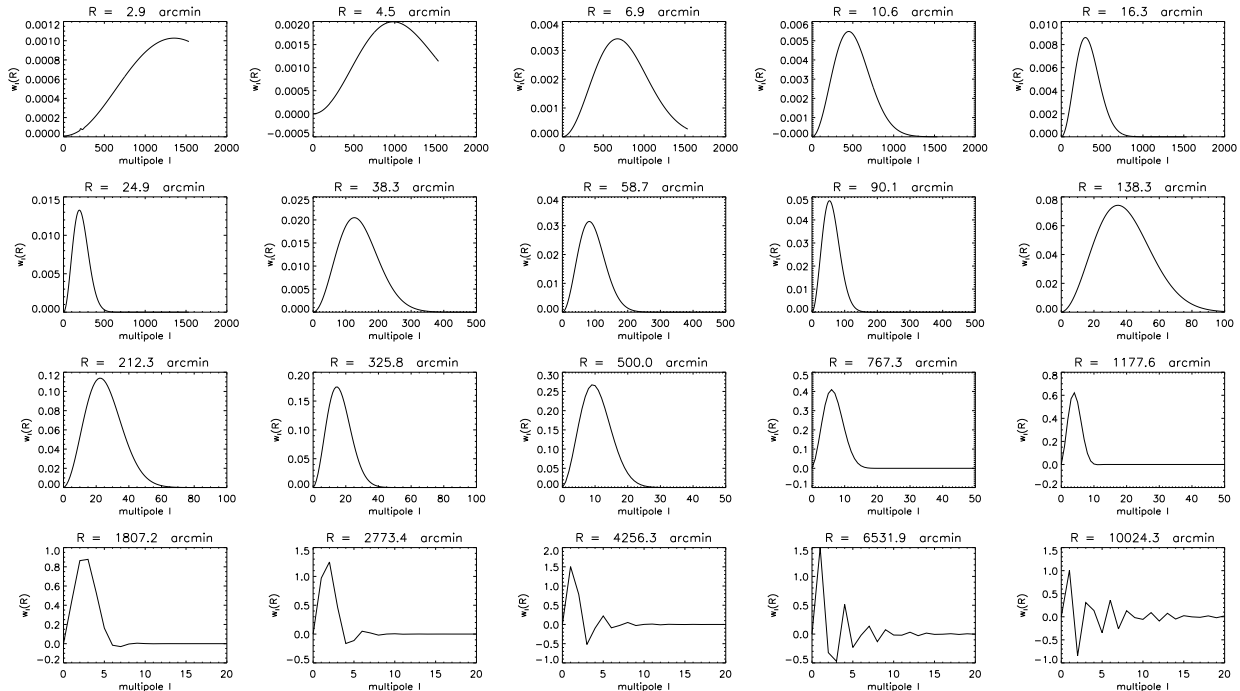
**Figure 5.** The window function of the SMHW for the list of selected angular scales for this case. We have convolved each wavelet window function with the pixel window function at $N_{side} = 512$. Note that the scales of 2.9 and 4.5 arc minutes are smaller than the pixel size (6.9 arc minutes). However they provide additional information because of the shape of the wavelet.

$\Omega_{cdm} = 0.25$, $\Omega_b = 0.05$, $\Omega_\Lambda = 0.70$, $\tau = 0.09$, $h = 0.73$ and $n = 1$. The variance of $f_{nl}$ is computed through the Fisher matrix of the bispectrum (see Eq. 28). We have used the gTfast code to estimate the radiation transfer function and evaluate the expected values of the local bispectrum for this experiment following Eq. (19) of Komatsu & Spergel (2001). We have computed $\sigma(f_{nl})$ for different $\ell_3 \leqslant \ell_{max}$ (see Fig. 4).

Note that as we include higher multipoles (i.e. smaller scales) $\sigma(f_{nl})$ decreases obtaining a limit of $\sigma(f_{nl}) = 5.4$ for $\ell_{max} = 1535$.

For the wavelet estimator, we consider the ideal experiment and the cosmological parameters defined previously for the primordial bispectrum estimators. To maximise the non-Gaussian signal we take a wide interval of different angular scales. We select 21 angular scales (including the unconvolved map) from 2.9 arc minutes to 167.07 degrees logarithmically spaced[4]. See Fig. 5 for the list of considered scales and the wavelet window function corresponding to these angular scales. We compute the third order quantities $\alpha_{ijk}$ given by Eq. 12 and the covariance matrix of the $q_{ijk}$ statistics given by Eq. 16 for these angular scales. There are

$(21+3-1)!/[3!(21-1)!] = 1771$ different third order statistics for 21 angular scales. The variance of $f_{nl}$ given by Eq. 20 and the variance estimated with Monte Carlo simulations require the inverse of the covariance matrix $C_{ijk,rst}$. This covariance matrix has a large condition number, defined as the ratio of the maximum and minimum eigenvalues. The eigenvalues of this matrix are plotted on the left panel of Fig. 6. This implies that the computation of its inverse is an ill-conditioned problem. Therefore the numerical errors present due to the limited precision of our computers (of the order of $2^{1-53} \simeq 10^{-16}$) can affect the value of $\sigma(f_{nl})$. In order to take into account the effect of this source of errors, we compute $\sigma(f_{nl})$ for different subsets of eigenvalues of the $C$ matrix using the PCA described in Subsect. 2.5. This is plotted on the right panel of Fig. 6 using the Fisher matrix for $f_{nl}$ given by Eqs. 24 and 25 and the PCA method. We as well plot the value of $\sigma(f_{nl})$ obtained with the Fisher matrix of the bispectrum given by Eq. 28 for the same experiment and $\ell_{max} = 1535$. In particular, imposing a limit on the ratio of the minimum and maximum eigenvalues of the covariance matrix $D_i/D_{max} \leqslant 10^{-12}$, we have $\sigma(f_{nl}) = 5.4$. Similar results are obtained for $\sigma(f_{nl})$ when it is estimated with $10^3$ Monte Carlo simulations. In particular, we have obtained $\sigma_{Fisher}(f_{nl})/\sigma_{sims}(f_{nl}) \simeq 0.93$ for the wavelet estimator. We have obtained a similar ratio for the bispectrum estimator in the same ideal experiment using the Fisher matrix and Gaussian simulations.

Finally, we have studied the dependence of the wavelet estimator on the angular scale. In Fig. 7 we present the $\sigma_{Fisher}(f_{nl})$ obtained with the wavelet estimator vs the $R_{min}$ and the $R_{max}$. We have used the PCA method in order to minimize the influence of the errors in the in-
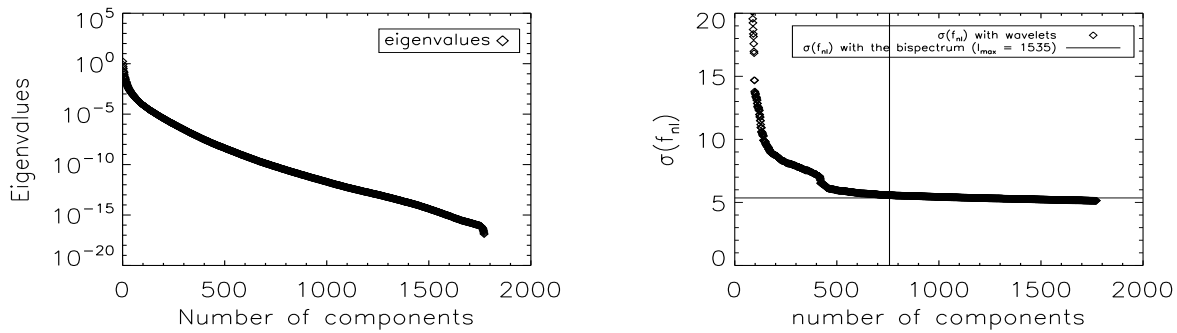
---

[4] The two smallest scales peak at very small angular scales, corresponding to sub-pixel structures at the selected resolution of $N_{side} = 512$. Although the localization properties of the wavelet may be affected for those scales for the considered resolution, we have checked that this effect does not affect the $f_{nl}$ estimation. To test this point, we have compared the values of $\sigma(f_{nl})$ using the same set of 21 angular scales in the current case of pixel resulution $N_{side} = 512$ and $\ell_{max} = 1535$ and in another case with $N_{side} = 1024$ and $\ell_{max} = 1535$. The differences in $\sigma(f_{nl})$ are $< 1\%$ between both cases.

**Figure 6.** *Left:* list of sorted eigenvalues of the covariance matrix $C$ among the list of 1771 third order statistics. *Right:* $\sigma(f_{nl})$ obtained with the wavelet estimator using different subsets of eigenvalues of the $C$ matrix following the PCA method. The vertical line shows the limit where the ratio of the maximum and minimum considered eigenvalues is $10^{12}$.
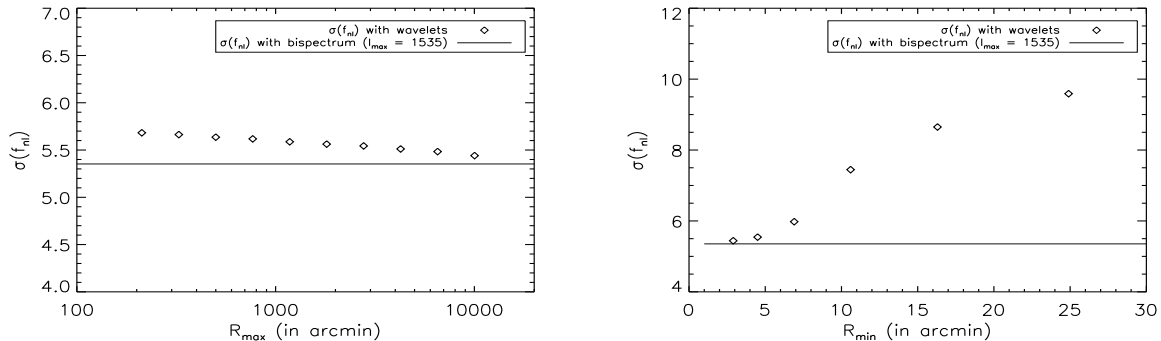


**Figure 7.** *Left:* $\sigma(f_{nl})$ vs the maximum angular scale $R_{max}$ considered for the analysis. *Right:* $\sigma(f_{nl})$ vs the maximum angular scale $R_{min}$ considered for the analysis.

verse of the $C$ matrix by using only the eigenvalues with $D_i/D_{max} \leqslant 10^{-12}$. We can see that $\sigma_{Fisher}(f_{nl})$ is highly dependent on $R_{min}$. This dependence is explained because the small scales map better the higher multipoles (even for scales smaller than the pixel size), while the large scales are all centered around low multipoles. We have also found that the most significant contribution to the local non-Gaussianity is given by combinations of small and large scales, which is in agreement with the squeezed configurations of the shape form of this kind of non-Gaussianity (see for example Fergusson & Shellard 2009; Jeong & Komatsu 2009).

### 3.2 Estimated error bars for $f_{nl}$ with a WMAP-like experiment

We have estimated the expected dispersion of the local $f_{nl}$ parameter for the WMAP 5-year data and WMAP 7-year data. In this analysis we have considered the instrumental properties of the experiment, the noise level and the recommended sky cuts of each data release. We have compared our results with the values obtained with the optimal estimator for WMAP 5-yr (Smith et al. 2009), where $\sigma(f_{nl}) = 21$, and with the optimal estimator for WMAP 7-yr (Komatsu et al. 2010) where $\sigma(f_{nl}) = 21$.

For WMAP 5-yr analysis we have used $10^4$ Gaussian simulations of the combined V+W WMAP 5-yr data to es-

timate the covariance matrix $C$ and 300 non-Gaussian simulations to estimate the expected values of the third order moments. We have normalised these non-Gaussian simulations to the $\Lambda$CDM model that best fits the WMAP 5-year data. As we are using a fraction of the full sky, we need to extend the masks in order to avoid the propagation of the zeros that are masking the Galaxy to other regions (Curto et al. 2009a), specially for large angular scales. This imposes a limit on the largest scale available for the analysis. In particular, from the set of scales given in Fig. 5, we use all the scales with at least 10% of the sky. Following the criteria to extend the masks defined in Curto et al. (2009a), we have 15 available scales. Their corresponding masked area is given in Table 1. In Fig. 8 we plot the eigenvalues of the $C$ matrix for this case and the $\sigma(f_{nl})$ for different subsets of eigenvalues of $C$ using the PCA method. Using $10^{12}$ as a safe limit for the ratio of the maximum and minimum eigenvalues, we obtain $\sigma(f_{nl}) = 22$ for this data. Compared with the optimal estimator based on the bispectrum (Smith et al. 2009), we obtain very similar results. Compared with the results presented by Curto et al. (2009a) and Curto et al. (2009b), we obtain significant improvements. The better results obtained here are explained because of the wider ratio of large-to-small angular scales considered now. This allows to have more third order moments with squeezed triangles for their corresponding three angular scales. These are the

**Table 1.** Considered angular scales and the fraction of the sky that is masked out by each extended mask for the WMAP 5-yr initial mask. Similar values are obtained for the WMAP 7-yr masks.

| index $i$ | 0 | 1 | 2 | 3 | 4 | 5 | 6 | 7 |
|---|---|---|---|---|---|---|---|---|
| scale $R_i$ | map | 2.9' | 4.5' | 6.9' | 10.6' | 16.3' | 24.9' | 38.3' |
| masked out area (%) | 28.4 | 28.4 | 28.4 | 28.8 | 29.3 | 29.9 | 30.7 | 31.8 |

| index $i$ | 8 | 9 | 10 | 11 | 12 | 13 | 14 | - |
|---|---|---|---|---|---|---|---|---|
| scale $R_i$ | 58.7' | 90.1' | 138.3' | 212.3' | 325.8' | 500' | 767.3' | - |
| masked out area (%) | 33.4 | 36.0 | 40.1 | 46.7 | 55.8 | 68.6 | 85.4 | - |
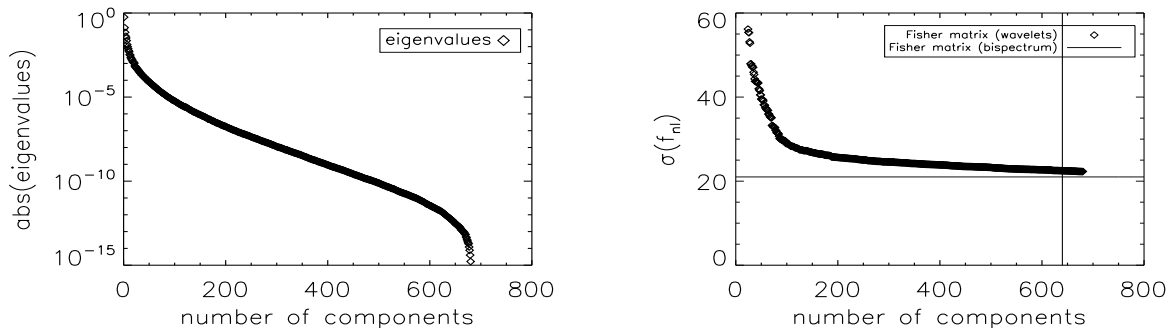


**Figure 8.** *Left:* list of sorted eigenvalues of the covariance matrix $C$ among the list of 680 third order statistics (15 scales) for WMAP 5-year data. *Right:* $\sigma(f_{nl})$ obtained with the wavelet estimator using different subsets of eigenvalues of the $C$ matrix following the PCA method. The vertical line shows the limit where the ratio of the maximum and minimum considered eigenvalues is $10^{12}$.

combinations where the most significant part of the local non-Gaussianity signal is located (Yadav & Wandelt 2010).

For the case of WMAP 7-year data, we have used $10^4$ Gaussian simulations of the combined V+W WMAP 7-yr data to estimate the covariance matrix $C$ and the same 300 non-Gaussian simulations normalised to the $\Lambda$CDM model that best fits WMAP 7-year data to estimate the expected values of the third order moments. We consider the same 15 angular scales as for the WMAP 5-year case masking a similar area. In Fig. 9 we plot the eigenvalues of the $C$ matrix for this case and the $\sigma(f_{nl})$ for different subsets of eigenvalues of $C$ using the PCA method. Using $10^{12}$ as a safe limit for the ratio of the maximum and minimum eigenvalues, we obtain $\sigma(f_{nl}) = 21$ for this data map. Compared with the optimal estimator based on the bispectrum (Komatsu et al. 2010), we obtain equally optimal error bars with the SMHW.

## 4   CONCLUSIONS

We have developed an efficient method to constrain the local $f_{nl}$ with the CMB anisotropies based on wavelets. We have found the dependence of the third order moments defined in Eq. 4 on $f_{nl}$ and the cosmological model through the primordial bispectrum (see Eq. 12). On the other hand we have found an analytical expression for the covariance matrix for all the third order statistics (see Eq. 16). Assuming a Gaussian-like distribution for the third order moments, we have estimated the variance of $f_{nl}$ through the Fisher matrix (see Subsect. 2.4). This variance is compared with the variance obtained with the same method for the bispectrum in Sect. 3. Both cases have been applied to an ideal

experiment with an angular resolution of 6.9 arcmin and without instrumental noise. After applying Principal Component Analysis in order to minimize the influence of the errors of the inversion of the covariance matrix, we have found that $\sigma(f_{nl}) = 5.4$ when we use the wavelets while $\sigma(f_{nl}) = 5.4$ for the bispectrum up to $\ell_{max} = 1535$. In addition, considering the case of a more realistic experiment with anisotropic and incomplete sky, such as the WMAP data, we have obtained $\sigma(f_{nl}) = 22$ for V+W WMAP 5-year data and $\sigma(f_{nl}) = 21$ for V+W WMAP 7-year data. These results are almost equal to the values obtained with the optimal bispectrum estimator where $\sigma(f_{nl}) = 21$ (Smith et al. 2009; Komatsu et al. 2010). All these results indicate that wavelets can be as efficient as the bispectrum to detect the non-Gaussianity of the local type. Apart from the efficiency of the tool (about 7 times faster than the bispectrum estimator for a WMAP-like experiment) it is remarkable that, as they are different statistical estimators, wavelets may be sensitive to different systematics in real data. Moreover wavelets allow us to test the isotropic character of the $f_{nl}$ parameter (Curto et al. 2009b; Rudjord et al. 2010) by studying different regions of the sky. We stress the importance of this statistical tool as an efficient alternative to measure local $f_{nl}$ in experiments such as Planck. In forthcoming works we will apply this tool on WMAP real data to constrain the local and other configurations of the non-linear coupling parameter $f_{nl}$.
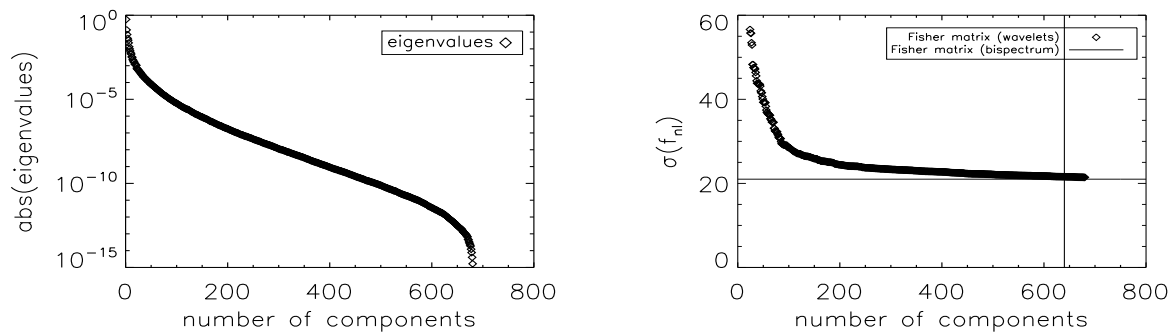
**Figure 9.** *Left:* list of sorted eigenvalues of the covariance matrix $C$ among the list of 680 third order statistics (15 scales) for WMAP 5-year data. *Right:* $\sigma(f_{nl})$ obtained with the wavelet estimator using different subsets of eigenvalues of the $C$ matrix following the PCA method. The vertical line shows the limit where the ratio of the maximum and minimum considered eigenvalues is $10^{12}$.

## REFERENCES

Albrecht A., Steinhardt P. J., 1982, Physical Review Letters, 48, 1220

Antoine J.-P., Vandergheynst P., 1998, Journal of Mathematical Physics, 39, 3987

Babich D., Creminelli P., Zaldarriaga M., 2004, Journal of Cosmology and Astro-Particle Physics, 8, 9

Bartolo N., Komatsu E., Matarrese S., Riotto A., 2004, Phys. Rep., 402, 103

Bucher M., Van Tent B., Sofia Carvalho C., 2010, MNRAS, 407, 2193

Cabella P., Pietrobon D., Veneziani M., Balbi A., Crittenden R., de Gasperis G., Quercellini C., Vittorio N., 2010, MNRAS, 405, 961

Casaponsa B., Barreiro R. B., Curto A., Martínez-González E., Vielva P., 2010, MNRAS, in press, arXiv:1009.0632

Cayón L., Martínez-González E., Argüeso F., Banday A. J., Górski K. M., 2003a, MNRAS, 339, 1189

Cayón L., Argüeso F., Martínez-González E., Sanz J. L., 2003b, MNRAS, 344, 917

Copi C. J., Huterer D., Schwarz D. J., Starkman G. D., 2006, MNRAS, 367, 79

Copi C. J., Huterer D., Starkman G. D., 2004, Phys. Rev. D, 70, 043515

Creminelli P., Nicolis A., Senatore L., Tegmark M., Zaldarriaga M., 2006, Journal of Cosmology and Astro-Particle Physics, 5, 4

Creminelli P., Senatore L., Zaldarriaga M., 2007, Journal of Cosmology and Astro-Particle Physics, 3, 19

Cruz M., Martínez-González E., Vielva P., Cayón L., 2005, MNRAS, 356, 29

Cruz M., Tucci M., Martínez-González E., Vielva P., 2006, MNRAS, 369, 57

Cruz M., Cayón L., Martínez-González E., Vielva P., Jin J., 2007a, ApJ, 655, 11

Cruz M., Turok N., Vielva P., Martínez-González E., Hobson M., 2007b, Science, 318, 1612

Cruz M., Martínez-González E., Vielva P., Diego J. M., Hobson M., Turok N., 2008, MNRAS, 390, 913

Cruz M., Vielva P., Martínez-González E., Barreiro R. B., 2010, arXiv:1005.1264

Curto A., Aumont J., Macías-Pérez J. F., Martínez-González E., Barreiro R. B., Santos D., Désert F. X., Tristram M., 2007, A&A, 474, 23

Curto A., Macías-Pérez J. F., Martínez-González E., Barreiro R. B., Santos D., Hansen F. K., Liguori M., Matarrese S., 2008, A&A, 486, 383

Curto A., Martínez-González E., Mukherjee P., Barreiro R. B., Hansen F. K., Liguori M., Matarrese S., 2009a, MNRAS, 393, 615

Curto A., Martínez-González E., Barreiro R. B., 2009b, ApJ, 706, 399

Dalal N., Doré O., Huterer D., Shirokov A., 2008, Phys. Rev. D., 77, 123514

de Oliveira-Costa A., Tegmark M., Zaldarriaga M., Hamilton A., 2004, Phys. Rev. D, 69, 063516

De Troia G., Ade P. A. R., Bock J. J., Bond J. R., Borrill J., Boscaleri A., Cabella P., Contaldi C. R., et al. 2007, ApJL, 670, L73

Desjacques V., Seljak U., 2010, Phys. Rev. D., 81, 023006

Dvali G., Gruzinov A., Zaldarriaga M., 2004, Phys. Rev.

D., 69, 023505

Elsner F., Wandelt B. D., 2009, ApJS, 184, 264

Eriksen H. K., Banday A. J., Górski K. M., Hansen F. K., Lilje P. B., 2007, ApJL, 660, L81

Eriksen H. K., Banday A. J., Górski K. M., Lilje P. B., 2005, ApJ, 622, 58

Eriksen H. K., Hansen F. K., Banday A. J., Górski K. M., Lilje P. B., 2004, ApJ, 605, 14

Fergusson J. R., Shellard E. P. S., 2009, Phys. Rev. D, 80, 043510

Frommert M., Enßlin T. A., 2010, MNRAS, 403, 1739

Górski K. M., Hivon E., Banday A. J., Wandelt B. D., Hansen F. K., Reinecke M., Bartelmann M., 2005, ApJ, 622, 759

Gott J. R., Colley W. N., Park C.-G., Park C., Mugnolo C., 2007, MNRAS, 377, 1668

Gruppuso A., Burigana C., 2009, Journal of Cosmology and Astro-Particle Physics, 8, 4

Guth A. H., 1981, Phys. Rev. D, 23, 347

Hansen F. K., Banday A. J., Górski K. M., 2004, MNRAS, 354, 641

Heavens A. F., 1998, MNRAS, 299, 805

Hikage C., Komatsu E., Matsubara T., 2006, ApJ, 653, 11

Hikage C., Matsubara T., Coles P., Liguori M., Hansen F. K., Matarrese S., 2008, MNRAS, 389, 1439

Hoftuft J., Eriksen H. K., Banday A. J., Górski K. M., Hansen F. K., Lilje P. B., 2009, ApJ, 699, 985

Jeong D., Komatsu E., 2009, ApJ, 703, 1230

Komatsu E., Spergel D. N., 2001, Phys. Rev. D, 63, 063002

Komatsu E., Wandelt B. D., Spergel D. N., Banday A. J., Górski K. M., 2002, ApJ, 566, 19

Komatsu E., Kogut A., Nolta M. R., Bennett C. L., Halpern M., Hinshaw G., Jarosik N., Limon M., Meyer S. S., Page L., Spergel D. N., Tucker G. S., Verde L., Wollack E., Wright E. L., 2003, ApJS, 148, 119

Komatsu E., Spergel D. N., Wandelt B. D., 2005, ApJ, 634, 14

Komatsu E., Dunkley J., Nolta M. R., Bennett C. L., Gold B., Hinshaw G., Jarosik N., Larson D., Limon M., Page L., Spergel D. N., Halpern M., Hill R. S., Kogut A., Meyer S. S., Tucker G. S., Weiland J. L., Wollack E., Wright E. L., 2009, ApJS, 180, 330

Komatsu E., Smith K. M., Dunkley J., Bennett C. L., Gold B., et al. 2010, arXiv:1001.4538

Liguori M., Matarrese S., Moscardini L., 2003, ApJ, 597, 57

Liguori M., Yadav A., Hansen F. K., Komatsu E., Matarrese S., Wandelt B., 2007, Phys. Rev. D, 76, 105016

Lin C., 2009, arXiv:0908.4168

Linde A. D., 1982, Physics Letters B, 108, 389

Linde A. D., 1983, Physics Letters B, 129, 177

Lyth D. H., Ungarelli C., Wands D., 2003, Phys. Rev. D, 67, 023503

Martínez-González E., Gallegos J. E., Argüeso F., Cayón L., Sanz J. L., 2002, MNRAS, 336, 22

Martínez-González E., 2008, arXiv:0805.4157

Matarrese S., Verde L., 2008, ApJL, 677, L77

Matsubara T., 2010, Phys. Rev. D, 81, 083505

Monteserín C., Barreiro R. B., Vielva P., Martínez-González E., Hobson M. P., Lasenby A. N., 2008, MN-RAS, 387, 209

Mukhanov V. F., Feldman H. A., Brandenberger R. H., 1992, Phys. Rep., 215, 203

Mukherjee P., Wang Y., 2004, ApJ, 613, 51

Natoli P., De Troia G., Hikage C., Komatsu E., Migliaccio e. a., 2009, arXiv:0905.4301

Pietrobon D., Cabella P., Balbi A., de Gasperis G., Vittorio N., 2009, MNRAS, 396, 1682

Pietrobon D., Cabella P., Balbi A., Crittenden R., de Gasperis G., Vittorio N., 2010, MNRAS, 402, L34

Rudjord Ø., Hansen F. K., Lan X., Liguori M., Marinucci D., Matarrese S., 2009, ApJ, 701, 369

Rudjord Ø., Hansen F. K., Lan X., Liguori M., Marinucci D., Matarrese S., 2010, ApJ, 708, 1321

Salopek D. S., Bond J. R., 1990, Phys. Rev. D, 42, 3936

Santos M. G., Heavens A., Balbi A., Borrill J., Ferreira P. G., Hanany S., Jaffe A. H., Lee A. T., Rabii B., Richards P. L., Smoot G. F., Stompor R., Winant C. D., Wu J. H. P., 2003, MNRAS, 341, 623

Sanz J. L., Herranz D., Lopez-Caniego M., Argueso F., 2006, arXiv:astro-ph/0609351

Seljak U., Zaldarriaga M., 1996, ApJ, 469, 437

Seljak U., 2009, Physical Review Letters, 102, 021302

Senatore L., Smith K. M., Zaldarriaga M., 2010, Journal of Cosmology and Astro-Particle Physics, 1, 28

Slosar A., Hirata C., Seljak U., Ho S., Padmanabhan N., 2008, Journal of Cosmology and Astro-Particle Physics, 8, 31

Smidt J., Amblard A., Serra P., Cooray A., 2009, Phys. Rev. D, 80, 123005

Smidt J., Amblard A., Byrnes C. T., Cooray A., Heavens A., Munshi D., 2010, Phys. Rev. D, 81, 123007

Smith K. M., Senatore L., Zaldarriaga M., 2009, Journal of Cosmology and Astro-Particle Physics, 9, 6

Smith S., Rocha G., Challinor A., Battye R. A., et al. 2004, MNRAS, 352, 887

Spergel D. N., Bean R., Doré O., Nolta M. R., Bennett C. L., Dunkley J., Hinshaw G., Jarosik N., et al. 2007, ApJS, 170, 377

Srednicki M., 1993, ApJL, 416, L1+

Verde L., Wang L., Heavens A. F., Kamionkowski M., 2000, MNRAS, 313, 141

Vielva P., Martínez-González E., Barreiro R. B., Sanz J. L., Cayón L., 2004, ApJ, 609, 22

Vielva P., Wiaux Y., Martínez-González E., Vandergheynst P., 2007, MNRAS, 381, 932

Vielva P., 2007, in Society of Photo-Optical Instrumentation Engineers (SPIE) Conference Series Vol. 6701 of Society of Photo-Optical Instrumentation Engineers (SPIE) Conference Series, Probing the Gaussianity and the statistical isotropy of the CMB with spherical wavelets

Vielva P., Sanz J. L., 2009, MNRAS, 397, 837

Vielva P., Martínez-González E., Cruz M., Barreiro R. B., Tucci M., 2010a, arXiv:1002.4029

Vielva P., Sanz J. L., 2010b, MNRAS, 404, 895

Wiaux Y., Vielva P., Martínez-González E., Vandergheynst P., 2006, Physical Review Letters, 96, 151303

Xia J., Viel M., Baccigalupi C., De Zotti G., Matarrese S., Verde L., 2010, ApJL, 717, L17

Yadav A. P. S., Wandelt B. D., 2008, Physical Review Letters, 100, 181301

Yadav A. P. S., Wandelt B. D., 2010, Advances in Astronomy, 565248